Journal of Power Sources 204 (2012) 25–33

Contents lists available at SciVerse ScienceDirect

Journal of Power Sources

journal homepage: www.elsevier.com/locate/jpowsour

The influence of discharge operation on the microstructure of strontium-doped lanthanum manganite cathode for solid oxide fuel cells

Jun Yang, Hiroki Muroyama, Toshiaki Matsui, Koichi Eguchi*

Department of Energy and Hydrocarbon Chemistry, Graduate School of Engineering, Kyoto University, Kyoto 615-8510, Japan

ARTICLE INFO

Article history:
Received 17 November 2011
Received in revised form
22 December 2011
Accepted 23 December 2011
Available online 2 January 2012

Keywords:
Solid oxide fuel cells
Strontium-doped lanthanum manganite
Cathode
Microstructure
Interface
FIB-SEM

ABSTRACT

In this work, discharge operation at a large current density was conducted for strontium-doped lanthanum manganite (LSM) cathodes, and the change in performance and microstructure of the interface between LSM cathode and YSZ electrolyte was investigated. For $(La_{0.8}Sr_{0.2})_{0.97}MnO_3$ (LSM97) with A-site deficiency, the performance was improved in the initial stage of discharge and then started to deteriorate continuously. The microstructural change in the interface between LSM97 and YSZ was quantitatively analyzed by using a dual-beam focused ion beam-scanning electron microscope. It was found that after discharge at 1.2 A cm^{-2} for 60 h, the surface of YSZ electrolyte was covered by a dense layer of LSM, accompanied with the formation of closed nanopores in the internal interface between LSM97 and YSZ. For $(La_{0.8}Sr_{0.2})_{1.03}MnO_3$ (LSM103) with a slight A-site excess, neither apparent formation of dense LSM103 layer along the LSM103/YSZ interface nor performance deterioration was observed during discharge. The mechanism for the structural change of LSM97 cathode was discussed based on the obtained results.

1. Introduction

Solid oxide fuel cells (SOFCs) are capable of providing clean energy by consuming hydrogen or hydrocarbon fuels at low environmental cost, of which cathode is one of the key components. Strontium-doped lanthanum manganite (LSM) is regarded as one of the most promising cathode materials for SOFCs because of high electrical conductivity, good thermal and chemical compatibility with other components, and high electrocatalytic activity for oxygen reduction reaction [1–6].

In addition to tremendous studies on the electrochemical behavior, the microstructural change of LSM-based cathodes, especially the interface between LSM cathode and YSZ electrolyte, has being attracting many attentions in recent years [7–12]. It was reported that the surface of YSZ electrolyte in contact with LSM or LSM/YSZ composite cathodes was significantly coarsened under polarization [9]. Miyoshi et al. detected the segregation of Mn-rich phase along the grain boundary of $LaMnO_3$ due to the change of oxygen nonstoichiometry [10]. Recently Matsui et al. quantitatively analyzed the microstructural change of the LSM–YSZ interface under cathodic polarization by using a dual-beam focused ion beam-scanning electron microscope (FIB-SEM). It was found that the YSZ surface was significantly coarsened even after 30 min of cathodic current treatment at 0.3 A cm^{-2} in O_2 at 1000 °C, accompanied with the formation of a large amount of closed pores along the LSM–YSZ interface [11]. However, these researches focused on the interfacial microstructural change of the LSM–YSZ interface in the initial stage of polarization at normal current densities (around 0.3 A cm^{-2}).

The change in microstructure of LSM-based cathodes during discharge operation could greatly affect the stability and durability of SOFC system. In this work, therefore, a long-term discharge operation was carried out on the cell at a relatively large current density. The microstructural change of the LSM–YSZ interface and its effect on the performance of LSM cathode under large current-loaded condition was investigated.

2. Experimental

The conventional electrolyte-supported cell of Ni/YSZ|YSZ|LSM was used. Commercial 8 mol% Y_2O_3-stabilized ZrO_2 disk (YSZ, Tosoh Corp; thickness: 500 μm, diameter: 24 mm) was used as the electrolyte. Ni/YSZ cermet with a volume ratio of Ni:YSZ = 68:32 was applied as an anode. The preparation procedure was described in our prevent work [13]. The strontium-doped lanthanum manganite cathodes with the formula of $(La_{0.8}Sr_{0.2})_xMnO_3$ at $x = 0.97$, 1.03 were denoted as LSM97 and LSM103, respectively. The content of the metal species was expressed in reference to Mn as unity. As a result, LSM97 and LSM103 represented A-site deficient and excess nonstoichiometry, respectively. The LSM powders were prepared by the acetate route. Corresponding metal acetates with required

* Corresponding author. Tel.: +81 75 383 2523; fax: +81 75 383 2520.
E-mail address: eguchi@scl.kyoto-u.ac.jp (K. Eguchi).

0378-7753/$ – see front matter © 2011 Elsevier B.V. All rights reserved.
doi:10.1016/j.jpowsour.2011.12.049

molar ratio were dissolved in deionized water and then dried at 120 °C. The resultant powders were calcined at 900 °C for 5 h. The as-prepared LSM powders were screen printed on the YSZ electrolyte and then fired at 1150 °C for 5 h. The formation of LSM97 and LSM103 was verified by X-ray diffraction and no secondary phase was observed. Platinum paste was painted to the side edge of the electrolyte and subsequently calcined at 900 °C in air for 2 h to serve as a reference electrode. The Ni/YSZ anode was reduced under hydrogen atmosphere at 1000 °C before the electrochemical measurements. Humidified hydrogen (95% H_2–5% H_2O) and pure oxygen were supplied to the anode and cathode with a flow rate of 100 mL min^{-1}, respectively.

Discharge operation was carried out at 1000 °C. During discharge operation at 1.2 A cm^{-2}, the terminal voltage of the cells with LSM97 and LSM103 cathodes remained between 0.25 V and 0.4 V. The value was extremely lower than that under the normal operating condition (0.7–0.9 V). The current was interrupted from time to time and electrochemical impedance spectroscopy (EIS) measurements were conducted under the open circuit state by using a Solartron 1260 frequency response analyzer and a Solartron 1287 electrochemical interface. The frequency range was from 100 kHz to 0.1 Hz and the signal amplitude was 10 mV.

The microstructure of the LSM–YSZ interface before and after discharge operation was investigated by scanning electron microscope (SEM, Nvision 40, Carl Zeiss-SIINT) equipped with energy-dispersive X-ray (EDX) spectrometer (Oxford). For comparison, the cell with LSM97 cathode held under the open-circuit state in pure oxygen at 1000 °C for 40 h was also investigated.

A dual-beam focused ion beam-scanning electron microscope (FIB-SEM, Nvision 40, Carl Zeiss-SIINT) was used for the three dimensional (3D) observation of the LSM–YSZ interface. The samples were buried in epoxy resin (Marumoto Struers KK) under vacuum conditions until solidified, and then cut and polished. The set of cross-sectional SEM images (*xy* plane) of the LSM/YSZ interface along the *z*-direction was obtained by sequential milling-and-observation operation. The phases of pore, LSM, and YSZ were distinguished by the contrast and the microstructures of them were three dimensionally reconstructed. The length of triple phase boundary (TPB) was also calculated. The respective phases were expanded slightly, and the TPB length was estimated from the overlapped region. Detailed descriptions of the 3D reconstruction and quantitative analysis of the LSM–YSZ interfacial microstructure are given in Refs. [11,12].

The composition of LSM near the LSM–YSZ interface was also investigated by energy-dispersive X-ray (EDX) spectrometer (JED-2300T, JEOL) in transmission electron microscope (TEM, JEM-2100F, JEOL). The sample for TEM analysis was buried in the resin overnight. Then the resin-buried sample was cut and polished with an abrasive paper into a rectangular bar of 2.8 mm × 2 mm × 100 μm. Subsequently the sample was reduced by Ar ion milling (EM-09100IS, JEOL) for electron transparency.

3. Results and discussion

3.1. Change in the performance of LSM cathodes during discharge operation

The typical change in terminal voltage and resistances of components for Ni/YSZ|YSZ|LSM97 during the discharge operation is shown in Fig. 1. When a current of 1.2 A cm^{-2} was loaded, the terminal voltage increased in the initial stage of 2 h, and then decreased continuously (Fig. 1a). The spiky drop of terminal voltage at 5, 10, 20, 30, and 40 h is due to current interruption for the impedance analysis. As can be seen in Fig. 1b, the change in the cell resistance was consistent with that in terminal voltage. In addition, the

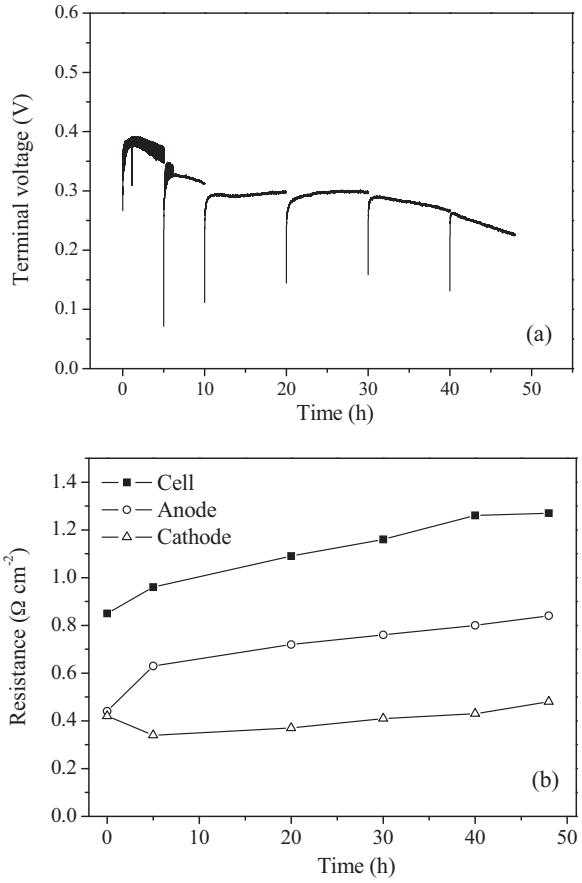

Fig. 1. Time courses of (a) terminal voltage and (b) resistances of the components for Ni/YSZ|YSZ|LSM97 during discharge operation at 1.2 A cm^{-2} for 48 h; temperature: 1000 °C. The resistance of each component consisted of ohmic and polarization resistances, obtained from EIS measurements.

deterioration of the Ni/YSZ anode largely contributed to the gradual decrease of the cell performance as compared with that of cathode.

More detailed investigation was carried out on another cell with LSM97 cathode. The change in the impedance spectra of LSM97 during discharge at 1.2 A cm^{-2} for 60 h is displayed in Fig. 2. The impedance spectrum of LSM97 before the current loading consisted of a large single semicircle. The intersection of the semicircle with the real axis at the high frequency gives the ohmic resistance (R_Ω). On the other hand, the polarization resistance (R_p) is defined as

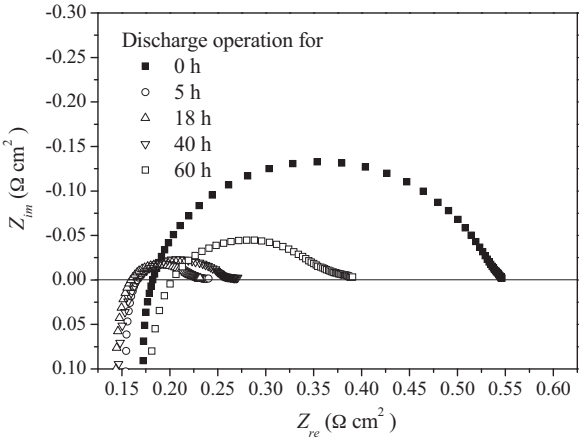

Fig. 2. Impedance spectra of LSM97 under the open-circuit state during discharge at 1.2 A cm^{-2} for 60 h; temperature: 1000 °C.

the distance between the x-intercept of the semicircle. Both R_Ω and R_p were reduced during initial 5 h, whereas they remained almost unchanged for another 13 h during continuous discharge. The performance improvement of LSM97 has been discussed in our previous work [13,14]. The formation of oxygen vacancies on LSM97 under cathodic polarization expanded the active sites for oxygen reduction reaction from TPB to its vicinity, and thus significantly enhanced the performance of LSM97 at the initial stage for 5 h, until the performance became stabilized. When a cathodic constant current was loaded, the oxygen vacancy concentration increased with time until a steady state was achieved. Thus, the impedance spectrum of LSM97 after discharge for 18 h was almost the same as that in 5 h. However, R_p of LSM97 increased after 40 h of discharge operation. Further current loading led to severe performance deterioration. Increases in both R_Ω and R_p of LSM97 were confirmed after discharge operation for 60 h.

3.2. Microstructural change in LSM97 over the YSZ electrolyte during discharge operation

The cross-sectional observation of the interface between LSM97 and YSZ before and after discharge is shown in Fig. 3. Before discharge, the porous layer of LSM97 was tightly adhered to the dense YSZ electrolyte (Fig. 3(a)). The LSM97 and YSZ oxides can be clearly separated from the contrast in the secondary electron image obtained by the in-lens detector (Fig. 3(b)). The composition of LSM97 was verified by EDX analysis. After discharge at 1.2 A cm^{-2} for 5 h, the morphology of the LSM97 particles was changed to form a thin layer of LSM on YSZ, as is designated by the white circle in Fig. 3(d). The prolonged discharge developed a dense layer of LSM with an approximate thickness of 1 μm on the YSZ electrolyte (Fig. 3(e)). However, a number of pores with a diameter of 50–200 nm appeared at the contact interface between LSM97 and YSZ. Further discharge led to the growth in thickness of the layer between LSM97 particles, as can be seen in Fig. 3(f). Neither the formation of secondary phase nor the significant metal elements diffusion through the interface was detected by EDX analysis. For comparison, the cell employing the LSM97 cathode was held under the open-circuit state at 1000 °C for 40 h, of which SEM images are shown in Fig. 3(g) and (h). No significant change in the microstructure of the annealed sample was observed as compared with the as-prepared one. Thus, it was concluded that the formation of the thin and dense layer between and the YSZ electrolyte in Fig. 3(c)–(f) resulted from the cathodic current loading.

The dense layer formed in the interface region after a long period of discharge operation was analyzed by TEM-EDX for the sample after discharge at 1.2 A cm^{-2} for 5 h was used. TEM image and mapping results of EDX analysis are displayed in Fig. 4. The newly formed layer was emphasized by the white ellipse in Fig. 4(a). La, Sr, and Mn components were distributed homogeneously in the bulk of LSM and the newly formed layer, as shown in Figs. 3 and 4(b)–(d). Fig. 4(e) and (f) revealed that Zr and Y elements were enriched locally in the newly formed layer. EDX spot analysis results in local compositions for the white-circle-selected areas in Fig. 5 are summarized in Table 1. At position 1–3, La, Sr, and Mn was observed as well as a large ratio of Zr and Y to Mn, whereas only Zr and Y elements were detected at position 4, which corresponds to Zr- and Y-rich region shown in Fig. 4. Based on these EDX analysis results, it is reasonable to consider that the newly formed layer resulted from the migration of LSM components on the YSZ surface. The observation of Zr and Y elements in the newly formed LSM layer will be due to the YSZ electrolyte underneath because the surface of YSZ electrolyte was significantly roughened under discharge operation. It is noted that the observed compositions in Table 1 are deviated from LSM97 and YSZ. Precise measurement of the amount of Sr and Y under the background of Zr by EDX is quite difficult because the peaks of the three elements in EDX spectrum are overlapped. Therefore, the results in Table 1 were semi-quantitative.

Table 1
EDX spot analysis results of the positions designated in Fig. 5.

Position	Mole ratio of the elements at each position designated in Fig. 5				
	La	Sr	Mn	Zr	Y
1	0.74	0.17	1.0[a]	0.42	0.02
2	0.84	0.27	1.0[a]	0.28	0.05
3	0.80	0.083	1.0[a]	0.20	0
4	0	0	0	0.89[a]	0.11

[a] The amount of Mn in position 1, 2, and 3 was assigned to unit; the sum of Zr and Y in position 4 was normalized to 1.

3.3. Quantitative analysis for the microstructure of the LSM97–YSZ interface by FIB-SEM

The migration of the LSM phase on YSZ as well as the formation of pores along the LSM97–YSZ interface could significantly affect the length of triple phase boundary (TPB), which serves as an active site in the cathode. Thus, the structural change of the LSM97–YSZ interface during discharge was quantitatively analyzed by FIB-SEM. Fig. 6 illustrates the 3D-reconstructed interface of LSM–YSZ before and after discharge under high current density of 1.2 A cm^{-2}. Since gaseous oxygen does not diffuse into closed pores, a part of TPB is inactive for the oxygen reduction reaction. TPBs open to the outer surface and those confined in the closed pores are defined as active and inactive TPBs. The visualized TPB lines over the YSZ surface obtained by computer processing are shown in Fig. 7. Before current passage, all the TPB was active for oxygen reduction reaction (Fig. 7(a)). The edge of the square in Fig. 7 was considered to connect to the atmosphere. As a result, TPB line connecting to the edge of the square was considered to be active for oxygen reduction reaction, otherwise it was inactive. After discharge for 5 h, many short lines of inactive TPB appeared, accompanied with disappearance of active TPB (Fig. 7(b)). Another 35 h of discharge led to a further increase in short branches of inactive TPB and a concomitant decrease in active TPB, as can be seen in Fig. 7(c).

The area-specific TPB length of LSM97 cathode before and after discharge is summarized in Table 2, which was obtained by dividing TPB length by area of YSZ surface and yz-plane, respectively.

The TPB length of the freshly prepared LSM97 sample, 1.08 μm μm^{-2}, was equal with the active one. This means that all TPBs were active and located in the open pores. After discharge for 5 h and 40 h, the TPB length did not decrease obviously, while the active TPB length was reduced to 0.49 μm μm^{-2} and

Table 2
Sample dimensions, spatial resolutions, and area-specific TPB length of LSM97 on YSZ after discharge at 1.2 A cm^{-2} for 0 h, 5 h, and 40 h; temperature: 1000 °C.

Discharge time (h)	Voxel size (nm)			Sample dimension (μm)		
	x	y	z	x	y	z
0	31.9	31.9	31.3	17.2	13.7	9.40
5	31.9	31.9	59.8	9.57	14.3	7.17
40	31.9	31.9	45.6	10.9	7.79	8.35

Discharge time (h)	Area-specific TPB length[a] (μm μm^{-2})	
	Total	Active
0	1.22	1.22
5	1.21	0.540
40	1.18	0.290

[a] Area-specific TPB length = TPB length (μm)/(area of yz plane, μm^2).

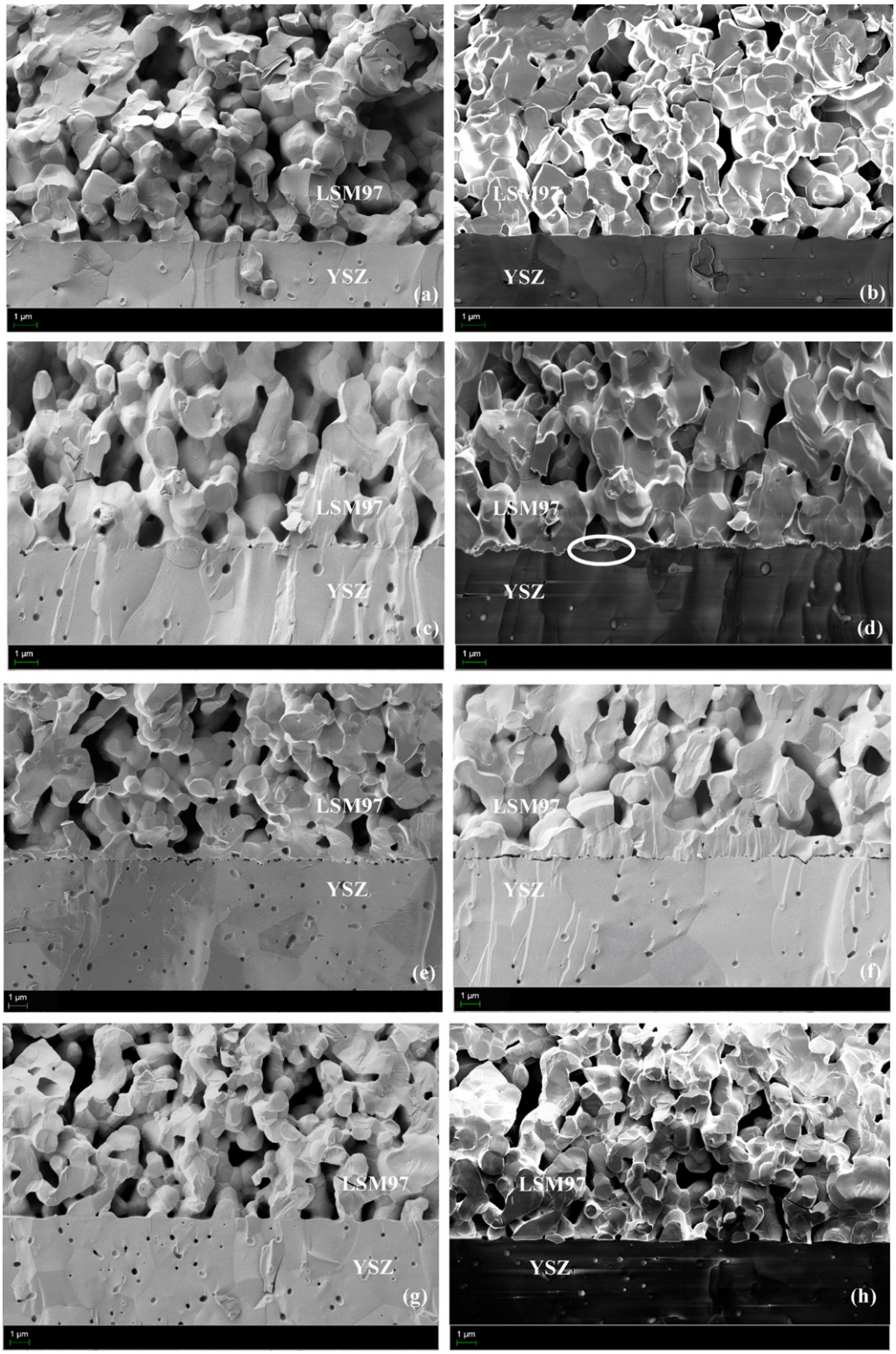

Fig. 3. Secondary electron images of LSM97 on YSZ (a), (b) after preparation and after discharge at 1.2 A cm^{-2} for (c) (d) 5 h, (e) 40 h, and (f) 60 h, and (g), (h) after holding in pure oxygen under the open-circuit state for 40 h at 1000 °C. The images were obtained by the chamber detectors for (a), (c), (e)–(g) and (b), (d), (h) by the in-lens detectors.

0.26 $\mu m\,\mu m^{-2}$, respectively. These data are consistent with the results in Fig. 7. The newly formed layer between LSM97 particles apparently reduced the TPB length. However, the nanopores at the LSM–YSZ interface gave rise to concomitant formation of many short and fragmented TPB lines, and therefore the overall TPB length was maintained. A large fraction of the pores newly formed during discharge were closed and inactive for the oxygen reduction reaction. Thus, the formation of the nanopores due to discharge was inefficient to promote the performance of LSM97 cathode, which agreed with the result reported by Matsui et al. [11].

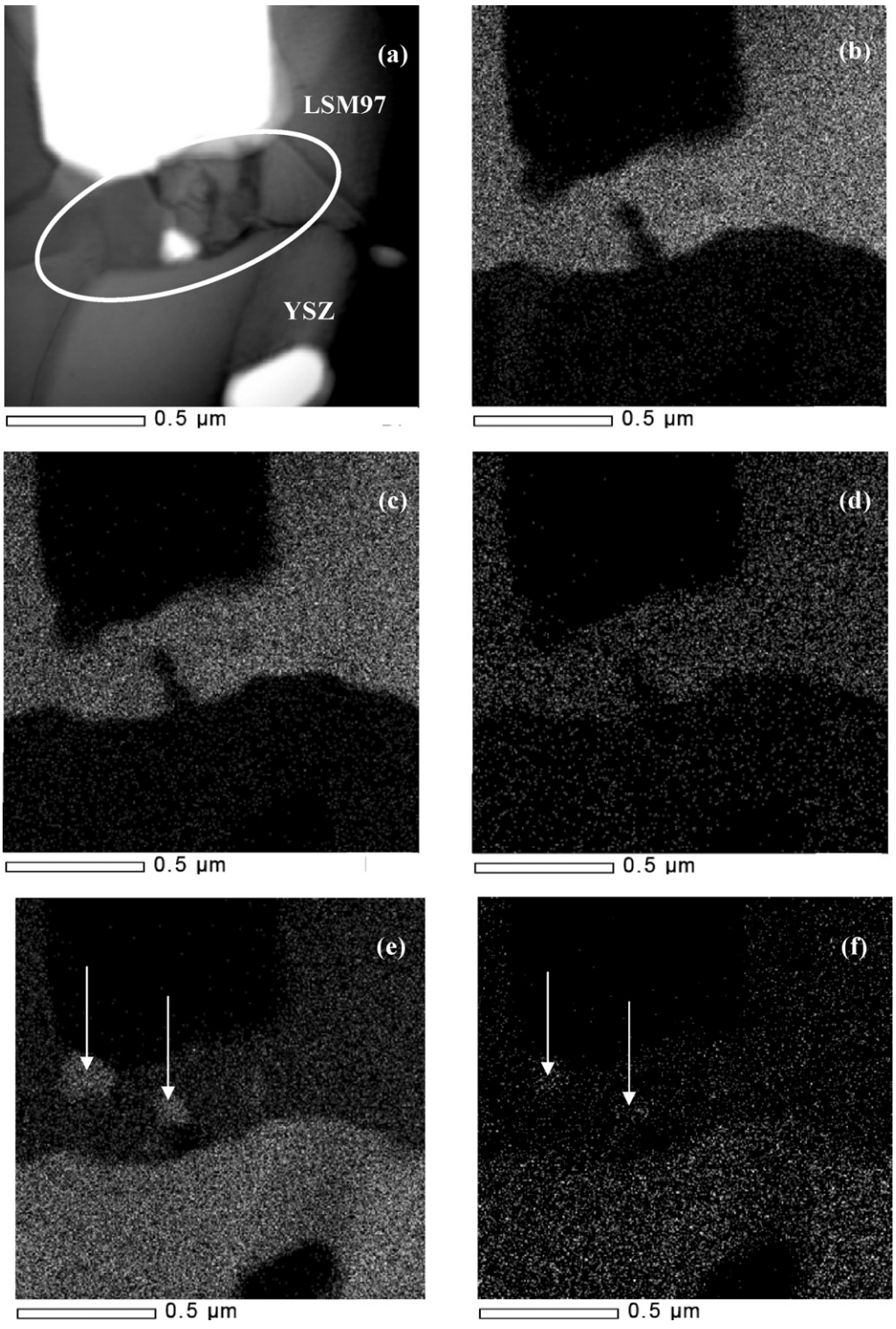

Fig. 4. (a) STEM bright field image of the newly formed layer on YSZ after discharge at 1.2 A cm^{-2} for 5 h; temperature: 1000 °C; EDX mapping for the same observation field as (a): (b) Mn mapping; (c) La mapping; (d) Sr mapping; (e) Zr mapping and (f) Y mapping.

Therefore, the porous LSM97 cathode was densified due to discharge operation. The change in the microstructure of LSM97 over YSZ can be concluded as follows:

(1) Before discharge, the porous LSM97 layer was tightly adhered to YSZ without nanosized pores at the interface. During discharge, the perovskite oxide tended to migrate from LSM97 particles onto the bare surface of YSZ, accompanied with the formation of nanosized pores at the LSM97–YSZ interface.
(2) The newly formed layer at the interface between LSM97 particles became thicker with time. After a long period of current loading, the YSZ surface was covered by the dense layer.

Although the active TPB length after 40 h of discharge was only 24% of that in the initial stage, the polarization resistance of LSM97

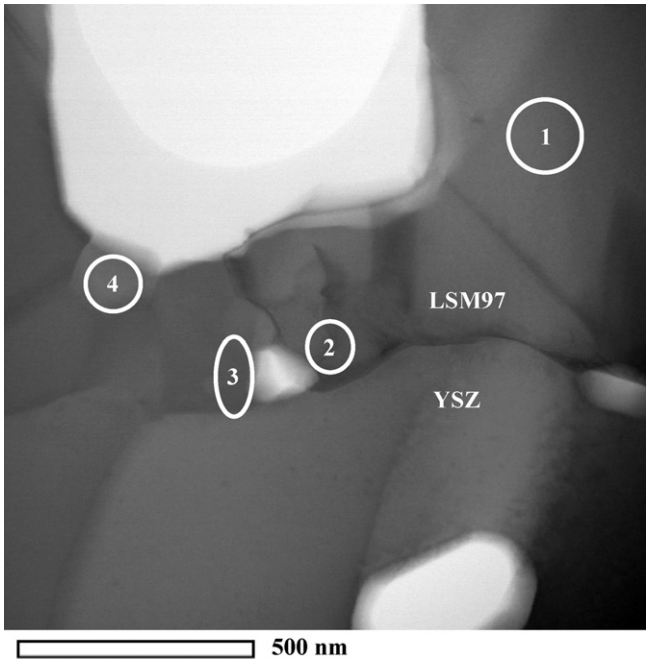

Fig. 5. STEM bright field image of the newly formed layer over YSZ after discharge at 1.2 A cm^{-2} for 5 h; temperature: 1000 °C. EDX spot analysis was conducted within the white circle-selected regions.

after discharge for 40 h observed from impedance spectrum in Fig. 2 was still smaller than that before discharge. This indicates that the change in the impedance of LSM97 during discharge operation cannot be explained simply by the change in the TPB length.

3.4. Microstructure for the LSM103–YSZ interface

Discharge operation was conducted in the same condition as in the previous sections for the cell with the LSM103 cathode. The behavior for impedance spectra of LSM103 was different from LSM97 as shown in Fig. 8. The impedance spectrum before current loading can be roughly deconvoluted into two semicircles: i.e., a small semicircle at the high-frequency region and a large one at the low-frequency region. The semicircle at the high-frequency region is attributed to the charge transfer process [7–9,15]. Because of the A-site excess nonstoichiometry of the LSM103 cathode, insulating phases, such as $La_2Zr_2O_7$ and $SrZrO_3$, are likely formed at the LSM103–YSZ interface of freshly prepared cell, resulting in the appearance of semicircle at high-frequency region. Since the A-site excess nonstoichiometry was only 0.03, the amount of the secondary phase was too small to be detected by SEM-EDX. The impedance of LSM103 decreased after discharge for 5 h. The performance enhancement of LSM103 can also be attributed to the formation of oxygen vacancies in the vicinity of TPB. After discharge for 40 h, ohmic resistance (R_Ω) remained almost unchanged while R_p kept decreasing. As a result, performance deterioration was not observed for LSM103 during 40 h of discharge operation at

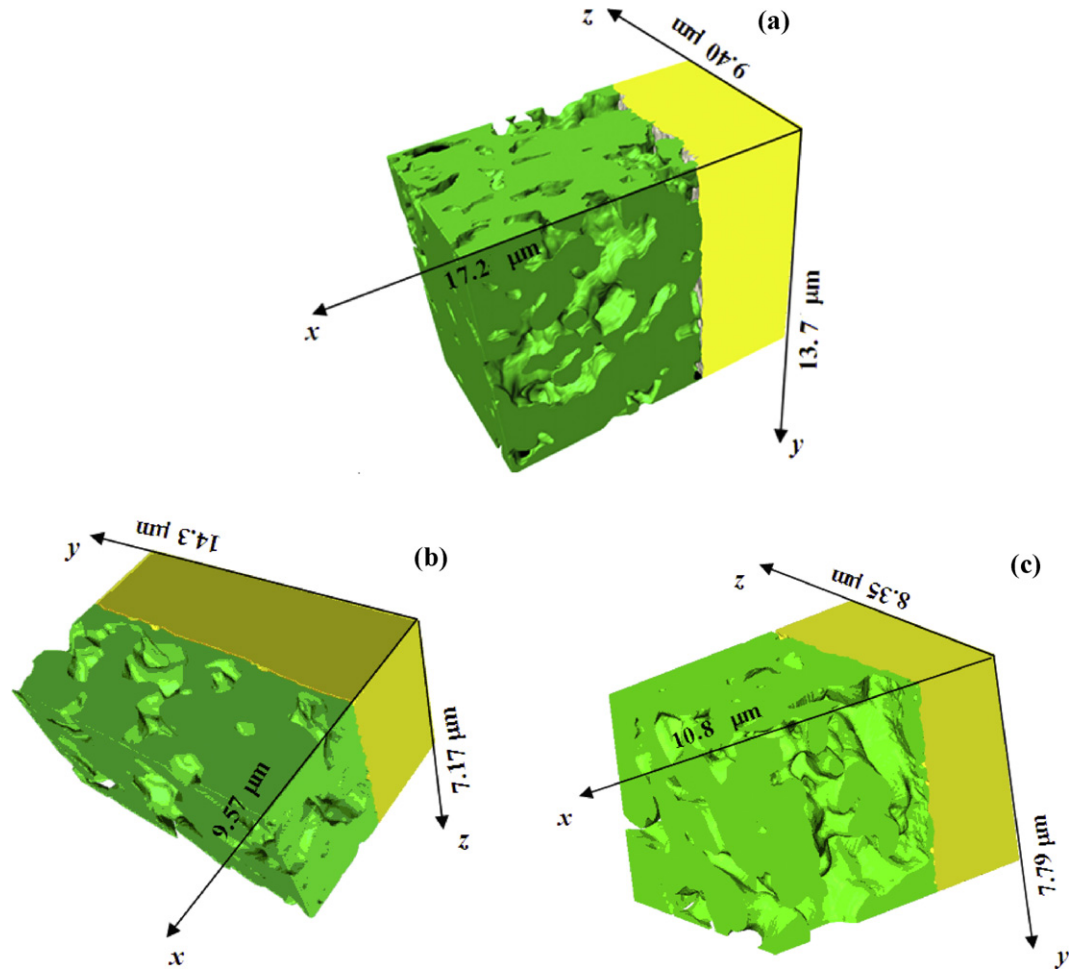

Fig. 6. 3D reconstructed LSM97 (green) on dense YSZ electrolyte (yellow) (a) before and (b, c) after discharge at 1.2 A cm^{-2} for (b) 5 h and (c) 40 h; temperature: 1000 °C. (For interpretation of the references to color in this figure legend, the reader is referred to the web version of the article.)

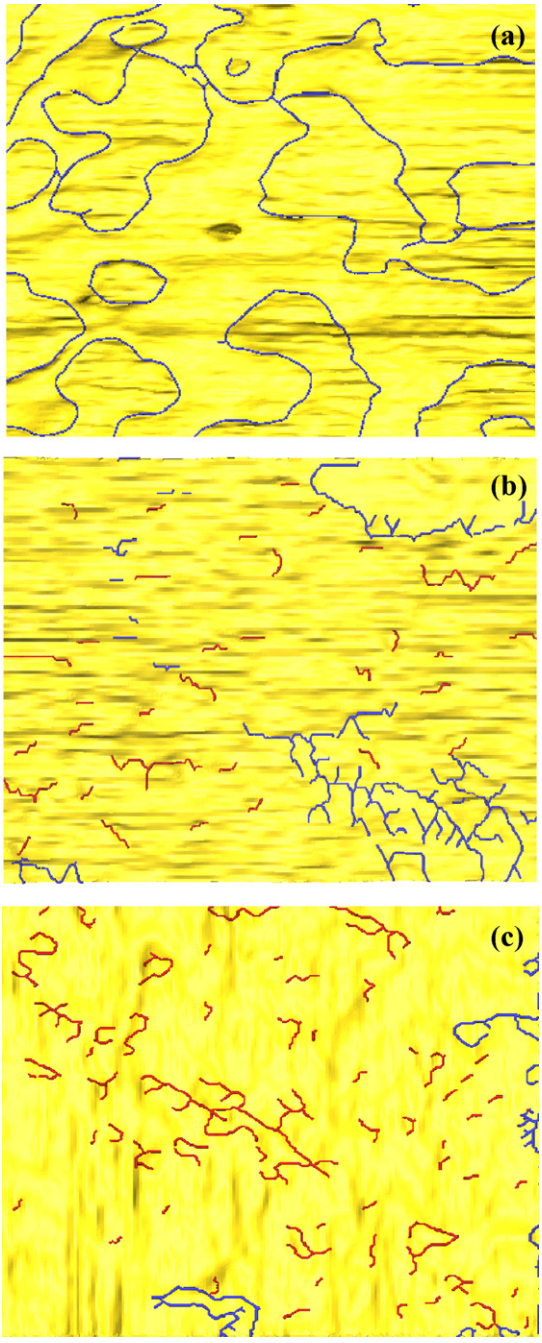

Fig. 7. Active (blue line) and inactive (red line) TPB lines on the surface of the YSZ electrolyte: (a) freshly prepared; (b, c) after discharge at 1.2 A cm^{-2} for (b) 5 h and (c) 40 h; temperature: 1000 °C. (For interpretation of the references to color in this figure legend, the reader is referred to the web version of the article.)

1.2 A cm^{-2}. Fig. 9 shows that even after discharge at 1.2 A cm^{-2} for 40 h, the YSZ electrolyte surface has not been totally covered by the thin layer. The densification, which was significant for LSM97, was suppressed in the case of the LSM103 cathode.

3.5. Mechanism for the densification of LSM97 cathode

According to the experimental results described above, it is reasonable to consider the densification of LSM97 cathode as the main reason for the performance deterioration during long-term discharge. The mechanism of the densification phenomenon described above is proposed as follows (see Fig. 10). At the beginning of

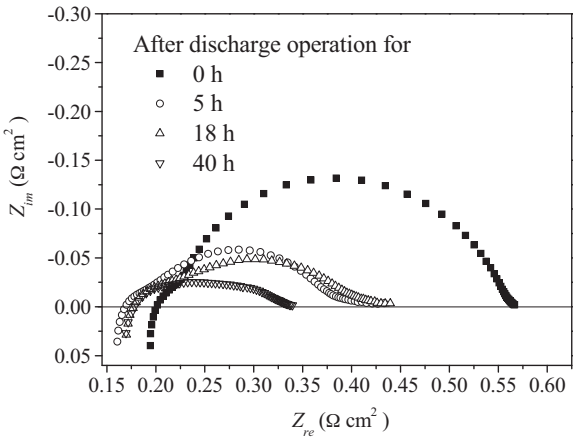

Fig. 8. Impedance spectra of LSM103 during discharge at 1.2 A cm^{-2}; temperature: 1000 °C.

discharge (see Fig. 10(a)), LSM97 particles contact well to YSZ without nanosized pores at the interface of LSM97 particles and YSZ. The contact region between LSM and YSZ excluding TPB is called as the internal LSM–YSZ interface. The reaction region at the triple phase boundary of LSM97, YSZ, and atmosphere (TPB) is depicted as the hatched area. Oxygen in the gaseous phase diffuses to the electrochemical active sites along TPBs via the LSM97 surface or

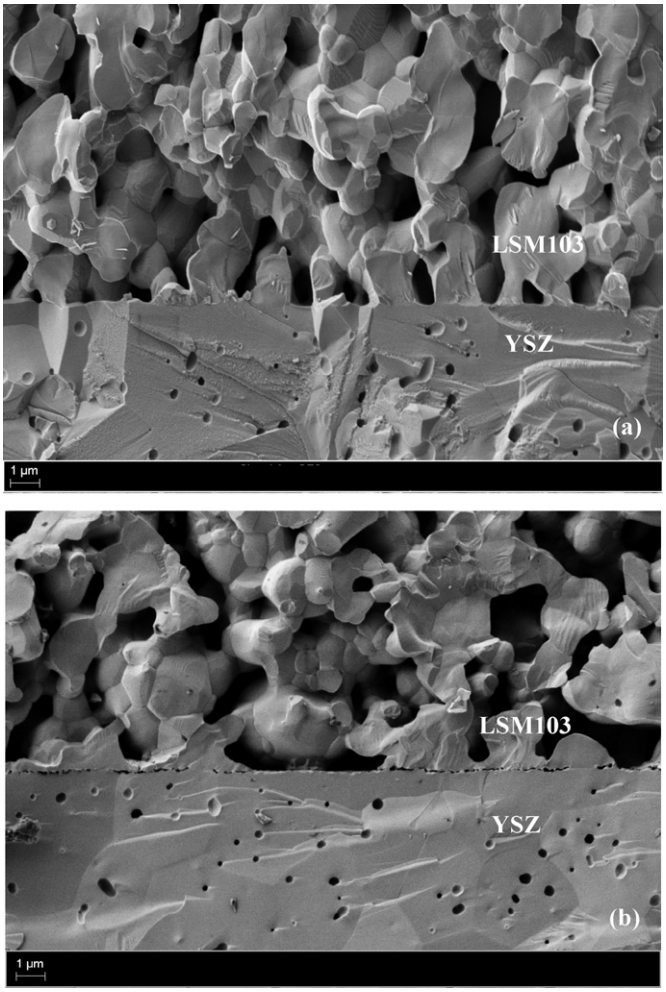

Fig. 9. Secondary electron images of LSM103–YSZ interface (a) before and (b) after discharge at 1.2 A cm^{-2} for 40 h; temperature: 1000 °C.

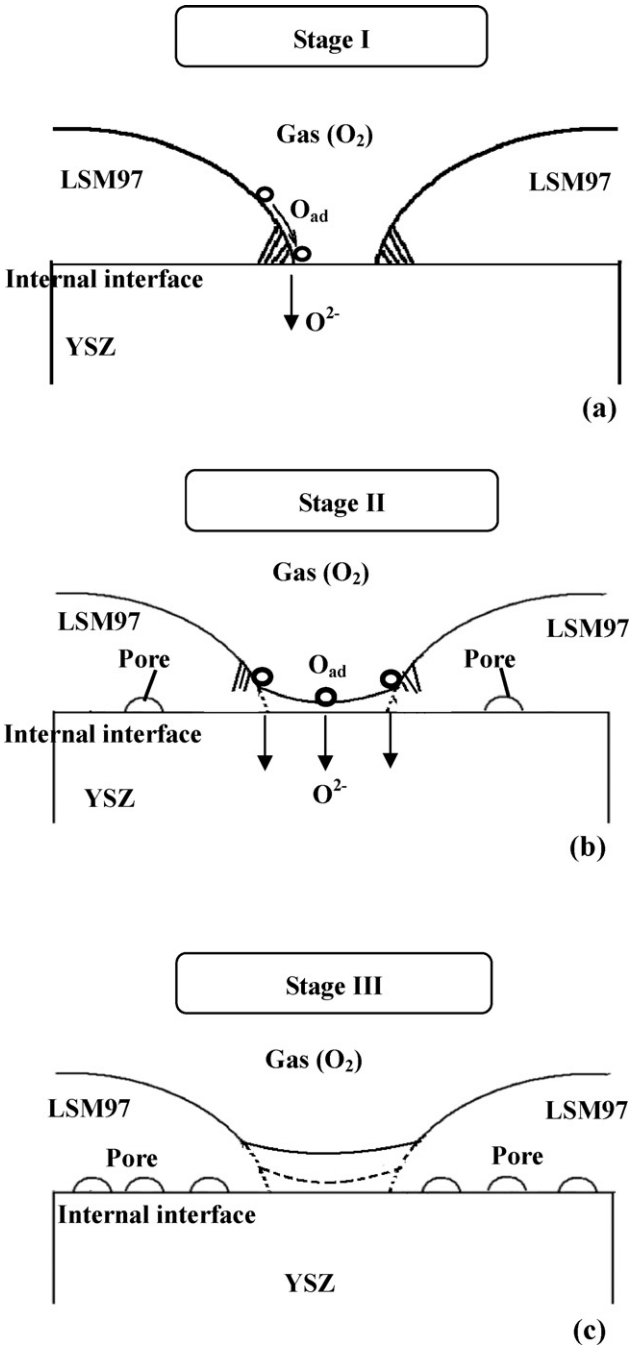

Fig. 10. Schematic illustration of the mechanism for the densification phenomenon of the LSM97 cathode during discharge operation.

gaseous channels to form oxide ions, which are then transported into the electrolyte. The LSM97 electrode is cathodically polarized during discharge. It is well accepted that LSM97 in the vicinity of the LSM97–YSZ interface tends to be reduced with the cathodic polarization, accompanied with the formation of oxygen vacancies. However, oxygen species can be hardly supplied to the internal interface of LSM97–YSZ, as LSM97 is almost pure electronic conductor at its original state. In contrast, oxygen species are continuous supplied to the TPBs and combine with oxygen vacancies. Thus the concentration of oxygen vacancies in the internal LSM97–YSZ interface is higher than that along the TPBs. Consequently, the concentration of metallic elements of LSM97 is relatively higher in the internal LSM97–YSZ interface than along the TPBs, driving metallic elements of LSM to diffuse from the internal LSM97–YSZ interface to the external TPBs. This leads to the formation of thin layer composed of La, Sr, and Mn elements on the YSZ surface and nanosized pores at the internal LSM97–YSZ interface (Fig. 10(b)). The newly formed thin layer contains La, Sr, and Mn elements, and can also be reduced, and therefore, ion conductive, with sufficient cathodic polarization. As a result, the active region for oxygen reduction reaction shifts from the TPB among LSM97–YSZ-gas phase to the polarized surface of thin LSM97 layer, facing to the gas phase. As a result, although the active TPBs of LSM, YSZ, and gas was reduced by the newly formed layer within the initial several hours of discharge, no significant degradation of LSM97 cathode can be observed in this stage.

However, the concentration gradient of oxygen vacancy developed from the internal LSM97–YSZ interface to the new reaction sites drives more metallic elements to migrate over the newly formed layer, resulting in the growth of the LSM layer and increase of nanopores along the internal LSM–YSZ interface (see Fig. 10(c)). After a sufficiently long period of discharge operation, LSM97 particles and the newly formed layer tightly cover the surface of YSZ. The layer between LSM97 particles eventually becomes so thick that the polarization resistance of the LSM cathode was enlarged by long-term discharge.

The suppression of the densification for LSM103 cathode may result from two factors. As discussed above, a small amount of secondary phase, such $La_2Zr_2O_7$ or $SrZrO_3$ may precipitate along the LSM103–YSZ interface. The secondary phase can obstruct the migration of metallic elements in LSM103 from the internal LSM103–YSZ interface to the triple phase boundary. The other explanation is that the A-site excess nonstoichiometry significantly reduces the concentration of metal vacancy, and thus slower the diffusion of metallic species in LSM103 and the morphological change of the cathode.

4. Conclusions

In this work, the accelerated microstructural change at the LSM–YSZ interface was intentionally induced during the long-term discharge operation at high current density. The porous LSM electrode with A-site deficient nonstoichiometry was densified at the LSM–YSZ interface during discharge operation at 1.2 A cm^{-2}. This phenomenon should be attributed to the migration of metallic elements of LSM from TPBs to the YSZ surface. Simultaneously, a large amount of closed nanosized pores were formed at the internal LSM–YSZ interface. These phenomena were responsible for the decrease in the active TPB length for oxygen reduction reaction. Consequently, the performance of the LSM cathode was deteriorated during long-term discharge operation. A slight excess nonstoichiometry at A-site of LSM significantly suppressed the migration of cations, and thus retarded the densification.

Acknowledgment

This work was supported by New Energy and Industrial Technology Development Organization (NEDO), Japan (Development of System and Elemental Technology on Solid Oxide Fuel Cell).

References

[1] E. Ivers-Tiffeĭe, A. Weber, D. Herbstritt, J. Eur. Ceram. Soc. 21 (2001) 1805–1811.
[2] J. Chen, F.L. Liang, B. Chi, J. Pu, S.P. Jiang, J. Li, J. Power Sources 194 (2009) 275–280.
[3] J.R. Wilson, J. Scott Cronin, A.T. Duong, S. Rukes, H.-Y. Chen, K. Thornton, D.R. Mumm, S. Barnett, J. Power Sources 195 (2010) 1829–1840.
[4] S.B. Sang, J. Pu, B. Chi, J. Li, J. Power Sources 193 (2009) 723–729.
[5] X.B. Chen, B. Hua, J. Pu, J. Li, L. Zhang, S.P. Jiang, Int. J. Hydrogen Energy 34 (2009) 5737–5748.
[6] F.L. Liang, J. Chen, S.P. Jiang, B. Chi, J. Pu, L. Jian, Electrochem. Commun. 11 (2009) 1048–1051.

[7] S.P. Jiang, W. Wang, Electrochem. Solid-State Lett. 8 (2005) A115–A118.
[8] X.D. Zhou, S.P. Simner, J.W. Templeton, Z. Nie, J.W. Stevenson, B.P. Gorman, J. Electrochem. Soc. 157 (2010) B643–B649.
[9] S.P. Jiang, W. Wang, Solid State Ionics 176 (2005) 1185–1191.
[10] S. Miyoshi, J.O. Hong, K. Yashiro, A. Kaimai, Y. Nigara, K. Kawamura, T. Kawada, J. Mizusaki, Solid State Ionics 154–155 (2002) 257–263.
[11] T. Matsui, Y. Mikami, H. Muroyama, E. Koichi, J. Electrochem. Soc. 157 (2010) B1790–B1794.
[12] H. Iwai, N. Shikazono, T. Matsui, H. Teshima, M. Kishimoto, R. Kishida, D. Hayashi, K. Matsuzaki, D. Kanno, M. Saito, H. Muroyama, K. Eguchi, N. Kasagi, H. Yoshida, J. Power Sources 195 (2010) 955–961.
[13] J. Yang, H. Muroyama, T. Matsui, K. Eguchi, J. Electrochem. Soc. 157 (2010) B449–B454.
[14] J. Yang, H. Muroyama, T. Matsui, K. Eguchi, Int. J. Hydrogen Energy 35 (2010) 10505–10512.
[15] W. Wang, S.P. Jiang, Solid State Ionics 177 (2006) 1361–1369.